Bulletin of the Seismological Society of America, Vol. 99, No. 4, pp. 2323–2334, August 2009, doi: 10.1785/0120080216

Ⓔ

Source Duration Scales with Magnitude Differently for Earthquakes on the San Andreas Fault and on Secondary Faults in Parkfield, California

by Rebecca M. Harrington and Emily E. Brodsky

Abstract We used a comparison of source time function pulse widths to show that a group of earthquakes on the San Andreas fault near Parkfield have a constant duration over a magnitude range of 1.4–3.7. Earthquakes on secondary faults have an increase in duration with magnitude, which is the expected relationship for the usual observation of constant stress drop. The constant duration suggests that fault area is the same regardless of magnitude and that variations in stress drop are due entirely to variations in slip. Calculated stress-drop values on secondary faults range from 0.31 to 14 MPa, and stress-drop values on the San Andreas fault range from 0.18 to 63 MPa. The observation of constant duration on the San Andreas fault is consistent with a model of a locked asperity in a creeping fault. The differences in durations between the events on the San Andreas fault and on secondary faults suggest that earthquakes on the San Andreas fault are inherently different. We speculate that faults with more cumulative displacement have earthquakes that may rupture differently. Furthermore, the differences in source properties between the two populations might be explained by differences in fault surface roughness.

Online Material: Station subsets used to evaluate cross-fault seismic velocity contrasts.

Introduction

In most tectonic environments, the duration of coseismic slip increases with average slip that occurs during rupture (Kanamori and Anderson, 1975). Both increasing slip and increasing fault length work in combination to increase seismic moment for large earthquakes. Moreover, the slip and the rupture length are directly proportional over large populations of earthquakes, independent of moment (Abercrombie, 1995; Ide *et al.*, 2003; Prieto *et al.*, 2004; Abercrombie and Rice, 2005; Imanishi and Ellsworth, 2006). A proportionality of slip and fault length implies an intimate link between the two. Both vary together with magnitude, and so any region with a broad distribution of earthquake magnitudes must have faults that can break at a variety of scales.

The implications of ordinary fault length-slip scaling is clear for large earthquake populations, but is it true for every faulting environment individually? Does the tectonic environment and faulting history predetermine the rupture length? If so, are earthquakes on some faults different than others? Observations of the Parkfield repeating earthquakes suggest that, in fact, some earthquakes are different than others (Nadeau and Johnson, 1998; Dreger *et al.*, 2007). Nadeau and Johnson (1998) observed that small patches of the San Andreas fault slip repeatedly with nearly identical earthquakes. The magnitude within a group of repeating events is the same, and the waveforms appear nearly identical. Therefore, on each repeating earthquake patch, the slip and fault length do not vary from earthquake to earthquake. This apparently unusual behavior may be related to the unusual tectonic locale of Parkfield at the transition from a creeping to locked fault and/or the extensive displacement of the mature San Andreas system (Titus *et al.*, 2005; Simpson *et al.*, 2006).

However, other earthquakes occur on the San Andreas fault in addition to the repeating events. The San Andreas fault near Parkfield has a fairly ordinary Gutenberg–Richter relationship over a magnitude range of approximately 2–6.5 (fig. 3 of Kagan, 1997), suggesting that there must be some variability of earthquakes. What controls this variability? Does the size of the slip patch vary with location on the fault surface? Here we take a close look at earthquake clusters that do not have identical magnitudes and that occur on different types of faults in efforts to elucidate the origin of the magnitude differences.

As an extremely well-instrumented area with both a plate-boundary fault and other secondary faults, Parkfield is an ideal location for comparing the source properties of earthquakes on faults with differing properties. We compare behavior on the mature San Andreas fault and the secondary fault structures in the region using the low-noise, high sample-rate borehole network. Using both an empirical Green's function method as well as raw data, we find that the magnitudes are, surprisingly, entirely determined by slip variability rather than covarying length and slip on the San Andreas fault.

We begin the article with a description of the data set and the method for determining source durations. In this section we will discuss how we approach removing path effects using an iterative deconvolution method. Next, we show in the Source Duration Observations section the observed differences between pulse widths of earthquakes on the San Andreas fault, and on secondary faults, using both the source time functions and the raw waveform data. Then, we show in the Source Spectral Observations section that the source spectra of earthquakes on the secondary faults have corner frequencies (and thus durations) that scale according to constant stress-drop values, while earthquakes on the San Andreas fault have durations that have little variation with increasing magnitude. In the Discussion section we show our calculations of stress drop ($\Delta\sigma$) and show how these quantities relate to seismic moment. We discuss the observations in the context of fault surface evolution in the Interpretation section.

Methods and Observations

Estimating source parameters accurately requires a good signal-to-noise ratio, ideally at many stations over a large bandwidth. Different techniques and different data often yield different results, and the energy estimates of various studies differ by sometimes as much as an order of magnitude (Singh and Ordaz, 1994; Venkataraman *et al.*, 2002). Given that we wish to compare subtle differences in the source spectra of comparably sized earthquakes, we only include earthquakes in our data set recorded on the same seismic stations, in order to more confidently rule out differences in the removal of site effects as a reason for any observed differences in source properties.

Ide *et al.* (2003) demonstrate that for small earthquakes the increase of source parameters, such as the ratio of radiated energy to seismic moment with earthquake magnitude, is more or less pronounced depending on the method used to account for the high-frequency path attenuation. We focus in this study on the dependence of source parameters on different faults, rather than the dependence on magnitude, but their results nevertheless highlight the importance of the method chosen for attenuation modeling. Their results indicate that using a constant Q-value to model attenuation produces apparent stresses that increase more dramatically with magnitude than when using spectral-ratio methods (which permit a nonconstant Q) to model attenuation. The discrepancy suggests at the very least that some of the size dependence is artificial and that methods using a constant Q underestimate radiated energy. The catalog magnitude of events in our data set ranges from M 1.4 to 3.7. A Brune spectral model with a complete stress drop predicts that our data set contains earthquakes with expected corner frequencies as high as approximately 20 Hz, making modeling attenuation at high frequencies particularly important (Singh and Ordaz, 1994). We therefore select a spectral-ratio approach as detailed subsequently.

Methods

Our data set includes 25 events located on the San Andreas fault and 11 earthquakes located on various secondary faults with magnitudes ranging from 1.4 to 3.7 (Table 1). We use the double-difference relocated catalog for Parkfield to obtain events located both on and off the active San Andreas fault strand, where those off of the main strand are assumed to be located on secondary faults (Thurber *et al.*, 2006; M. J. Rymer, personal comm., 2007). Earthquakes located on the main fault strand are termed on-fault, and those located off the main strand are termed off-fault (Figs. 1 and 2).

Because we obtain source time functions via a spectral division method, we are limited to colocated event pairs with a magnitude unit or more difference in size. The locations of the off-fault clusters are dictated primarily by data availability. We have done an exhaustive search for event pairs located within 300 m of one another in the relocated catalog of Thurber *et al.* (2006), and the pairs studied are the only suitable candidates. The distances of the on-fault clusters are chosen to range from the center of the station array up to distances comparable to the off-fault events.

We select our off-fault event pairs for the deconvolution by choosing clusters of earthquakes over 5 km from the main San Andreas fault trace with a minimum size difference of at least one magnitude unit (Fig. 1). Studies of fault-zone guided waves estimate that the width of the San Andreas fault at Parkfield is less than 200 m (Li *et al.*, 1997). We choose a minimum distance of 5 km because it gives us confidence that the off-fault events are on secondary faults, rather than additional, active strands of the San Andreas fault system.

The waveforms are provided by the Berkeley Seismological Laboratory, University of California, Berkeley, which operates the Parkfield High Resolution Seismic Network (HRSN) via the Northern California Earthquake Data Center (NCEDC). The HRSN consists of 13, three-component borehole stations with depths ranging from 63 to 572 m, an average depth of 236 m, and a sampling rate of 250 samples/sec (see the Data and Resources section).

The first step is to use the entire waveform of each earthquake in our data set to deconvolve the empirical Green's function from the larger colocated event in order to obtain the source time function at each station. We chose the projected Landweber deconvolution method, which is a regularizing, constrained, iterative approach to empirical Green's

Table 1
Earthquakes Considered in This Study (Taken from the Catalog of Thurber *et al.*, 2006)

Date (yyyy/mm/dd)	Time (UTC)	Latitude (°)	Longitude (°)	Depth (km)	Magnitude	Event ID	τ (msec)	f_c (Hz)
2004/09/05	07:05:04.86	35.7685	−120.319	8.369	1.6	21393520	56.0	14.4
2004/09/28	17:57:43.98	35.7784	−120.33	8.388	2.7	21400463	75.6	15.6
2004/09/28	19:40:23.6	35.7785	−120.33	8.649	2.9	21400518	62.5	16.1
2004/09/28	20:55:07.64	35.7818	−120.323	4.161	2.1	51148134	77.8	15.0
2004/09/28	21:49:23.56	35.7771	−120.329	8.575	2.9	21400488	103.6	7.4
2004/09/28	21:57:37.88	35.7983	−120.342	4.163	2.1	51148203	68.4	15.0
2004/09/29	18:59:59.92	35.7827	−120.334	8.328	2	51148847	68	15.2
2004/09/30	01:57:50.06	35.7812	−120.323	3.97	1.7	21400936	81.2	16.2
2004/10/07	14:32:03.64	35.781	−120.332	8.593	2.3	51150206	77.5	12.0
2004/10/18	06:22:57.07	35.7826	−120.334	8.192	2	51151460	66.9	14.9
2004/10/18	06:27:51.91	35.7822	−120.334	8.279	1.7	51151464	59.6	14.5
2004/10/19	15:52:17.48	35.7699	−120.321	8.619	2.1	51151568	61.1	14.6
2004/10/20	09:09:47.86	35.7978	−120.341	4.268	2.4	51151627	70.0	14.7
2004/10/29	03:32:43.73	35.781	−120.333	8.751	3.3	21415362	88.7	13.4
2004/11/03	14:42:54.09	35.7667	−120.318	8.324	1.6	21416910	60.0	4.5
2001/09/20	20:06:02.64	35.9347	−120.487	5.261	2.2	21194856	38.8	20.9
2004/09/28	18:37:16.76	35.9345	−120.487	5.216	1.7	51148006	39.2	19.3
2004/09/28	23:33:49.64	35.9347	−120.487	5.272	2.4	21400519	41.2	18.3
2004/10/02	23:25:08.72	35.9354	−120.487	5.349	2.5	51149613	39.6	18.5
2005/01/08	04:46:6.00	35.9346	−120.487	5.27	2.4	21432539	48.0	18.2
2004/02/04	14:29:57.39	36.0951	−120.66	7.518	1.4	21340072	44.0	24.8
2005/02/09	10:45:23.62	36.095	−120.66	7.518	2	21438412	58.5	20.4
2005/02/09	10:53:15.6	36.0953	−120.66	7.527	1.4	21438414	51.6	16.8
2006/03/11	08:25:42.98	36.0362	−120.596	4.82	2.41	21508986	66.8	13.5
2007/01/17	10:11:35.6	36.037	−120.595	4.83	2.25	51177776	60.7	17.9
2002/06/04	22:33:56.28	35.932	−120.676	10.163	2.3	21228776	32.5	23.5
2002/06/04	22:50:02.08	35.932	−120.676	10.168	2.3	21228784	53.2	16.6
2004/09/06	03:43:04.43	36.148	−120.653	4.398	2.8	21393628	92.4	6.1
2004/09/26	15:54:05.96	36.143	−120.666	4.48	3.7	21399972	175.5	4.8
2004/09/27	08:52:40.96	36.154	−120.658	4.821	2.8	21400160	81.1	9.7
2004/09/27	10:38:56.32	36.152	−120.658	4.32	2.3	21400192	78.8	12.2
2004/10/03	02:11:15.36	36.153	−120.658	4.347	2.8	21402827	74.0	13.7
2006/06/27	21:38:11.87	36.065	−120.192	16.95	3.19	21524551	103.9	8.7
2006/12/15	19:50:25.33	36.170	−120.298	9.96	2.41	51176831	108.6	9.7
2007/03/12	12:13:54.63	35.938	−120.691	8.89	2.06	40194471	25.6	31.6
2007/09/20	05:41:07.00	36.064	−120.194	14.34	2.32	40202213	160.6	8.8

The 25 events located on the San Andreas fault are grouped into the three clusters from southeast to northwest (Fig. 1). Each cluster is separated by a single line. The 11 events located on secondary faults (bottom rows of the table) are separated by a double horizontal line. Duration is taken as the width of the source time pulse, and corner frequencies are determined using the source time function and a least-squares fit to a Brune spectral model.

function deconvolution, and is outlined in detail in Lanza *et al.* (1999). The method imposes a positivity constraint on the solution and is therefore particularly well suited for determining signals that may be assumed to be positive, such as the displacement on a fault. We refer the reader to Lanza *et al.* (1999) for further details.

Once we obtain the source time function at all stations, we measure the pulse width directly and calculate the source spectra of each event. We use the source time function to measure pulse width as a proxy for source duration (τ) and then calculate the corner frequency (f_c) via a least-squares fit to a Brune spectral model. We also measure the pulse widths of the direct P-wave arrival for the on-fault events and calculate an average pulse width using all stations. We will discuss in the Source Duration Observations section why we measure the pulse widths of the on-fault events using the direct P-wave arrival in addition to the source time function. Pulse width is inversely proportional to f_c, but it does not require a source model to quantify it. For each event, we stack all of the available source time function files determined at each station in order to have a spatially averaged source time function. We then take the width of the source time pulse at $1/2$ of the peak pulse amplitude value as τ for the off-fault events. We use the width of the pulse at $1/2$ the peak amplitude in order to avoid mistakenly interpreting noise or leakage from the deconvolution process as extended source duration.

Only the on-fault cluster in the middle of the array has complete azimuthal coverage. We attempt to alleviate radiation pattern effects resulting from sampling only part of the focal sphere for the off-fault earthquakes by choosing events at varying azimuths relative to the array. Some error

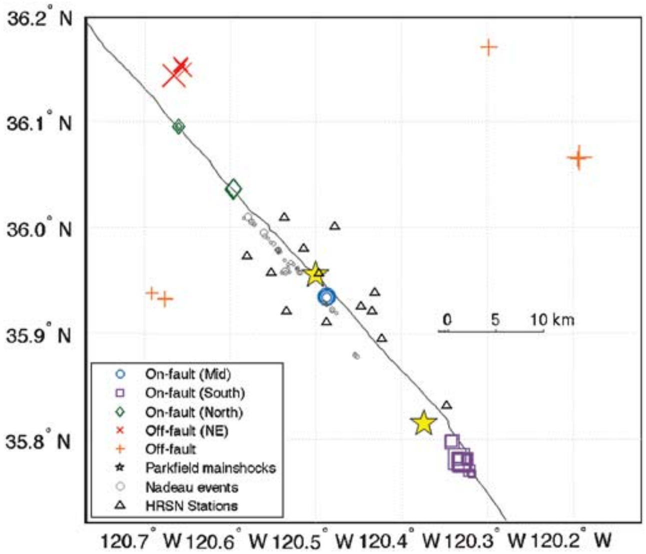

Figure 1. Study area: the map shows the location of the on-fault (blue circles, purple squares, and green diamonds) and off-fault (orange crosses and red Xs) events used in our study. Markers are scaled according to earthquake magnitude. The gray circles indicate the location of the repeating earthquakes studied by Nadeau and Johnson (1998). Source time functions for these earthquakes are obtained by projected Landweber deconvolution of a colocated earthquake that is at least one magnitude unit smaller than the events shown. The large yellow stars represent the epicenters of the 1966 and 2004 earthquake epicenters.

in calculated duration for both the off-fault events and the remaining on-fault events will be introduced by not having complete azimuthal coverage. However, we show in subsequent sections that we observe the expected scaling between

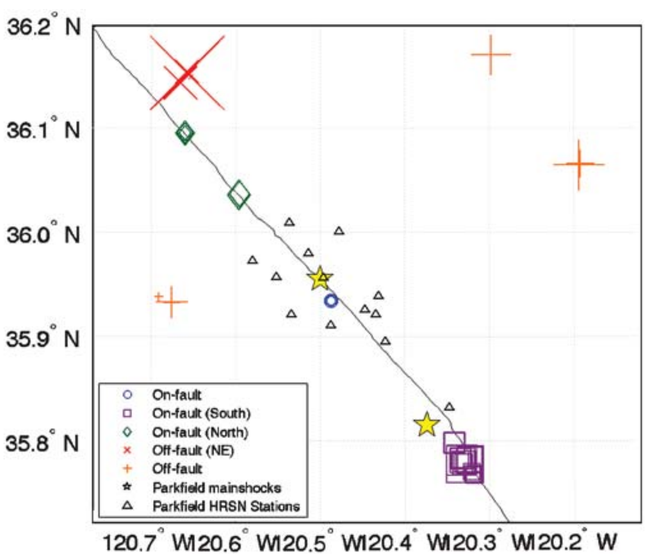

Figure 2. Study area: the map shows the location of the on-fault (blue circles, purple squares, and green diamonds) and off-fault (orange crosses and red Xs) events used in our study. The markers are scaled according to the source duration as determined from the source time function pulse width. Source spectra and source properties of the events are shown in subsequent figures with the same color/symbol scheme.

moment and duration assuming a constant stress drop for events on secondary faults and calculate stress-drop values ranging from 0.31 to 14 MPa. The calculated values fall well within accepted values of stress drop (Abercrombie, 1995). Furthermore, we performed the same analysis for each of the event pairs first using only stations northeast of the fault and again using stations southwest of the fault, in order to establish if the changing geology across the fault affected the results. Only negligible differences between the two groups of stations exist (Ⓔ auxiliary Figs. 1 and 2, available in the electronic edition of *BSSA*). We will show that both the empirical Green's function deconvolution, as well as the raw waveforms, indicate that source durations for the events on the San Andreas fault effectively do not vary over the magnitude range observed. The calculated durations for the remaining on-fault events agree with those results for the cluster in the middle of the array, suggesting that the coverage is sufficient for the purposes of measuring pulse durations.

In addition, both on- and off-fault earthquakes are chosen at a variety of azimuths and at comparable distances from the center of the array in order to confidently rule out any observable differences between spectral shapes as being the effect of attenuation or radiation pattern. We choose such a variety of events merely as a precautionary measure, as the empirical Green's function deconvolution should, in theory, remove any path effects (Nakanishi, 1991; Hough, 1997).

We calculate the source time spectra of the off-fault events at each station by using files with 1 sec windows around the peak of the source time function pulse (specifically 512 points). We calculate a root mean square spectral amplitude using the multitaper method provided by the MATLAB multitaper function using all three components. Finally, we average the spectral values at all stations to calculate one spectrum for each event. We model the long-period amplitude (Ω_0) and the corner frequency (f_c) of each single spectrum via a least-squares fit to a Brune spectral model with spectral fall off of $n = 2$ (Brune, 1970; Abercrombie, 1995). Allowing n to vary in the spectral calculation did not significantly increase the fit. We therefore infer that the spectral fall off follows the expected value of $n = 2$ and that the regularized source time function calculation does not significantly affect the fall off,

$$\Omega(f) = \frac{\Omega_0}{(1 + (\frac{f}{f_c})^n)}. \qquad (1)$$

The modeled long-period spectral amplitude is equal to a spectral ratio. Many of the earthquakes in the data set do not have a common empirical Green's function, making relative long-period amplitude (and hence magnitude) comparisons impossible. We therefore scale the spectra to their expected long-period amplitude values (inferred from catalog magnitudes) by multiplying by a constant equal to the ratio of the expected long-period amplitude to the spectral-ratio long-period amplitude. Scaling the spectra in this way invokes an implicit assumption that catalog magnitudes are accurate and that the magnitude scale used scales with seismic moment similarly to moment magnitude (M_w).

We test the validity of the assumption by comparing the magnitudes of events within a single cluster with the relative amplitudes of the source time functions (Fig. 3).

As discussed previously, each cluster uses the same empirical Green's function, so the relative source time amplitude is a measure of the relative seismic moment. The amplitude of the source time function, A, is proportional to moment rate, which can be approximated as moment divided by duration, τ,

$$A(t) \propto \dot{M}_0 \propto \frac{M_0}{\tau}. \quad (2)$$

For earthquakes with stress drops independent of magnitude, the duration scales with the moment as follows (Kanamori and Anderson, 1975):

$$M_0 \propto \tau^3. \quad (3)$$

(We will relax the constant stress-drop assumption later in this article.) Substituting τ in terms of M_0 from equation (3) into the expression on the right in equation (2) and combining with the assumed magnitude moment relations gives us

$$M_0 = 10^{1.5(M+6.07)}, \quad (4)$$

where moment has units of newton meters (Kanamori and Anderson, 1975). Using equations (2) and (4) we derive a relationship between source pulse amplitude and magnitude,

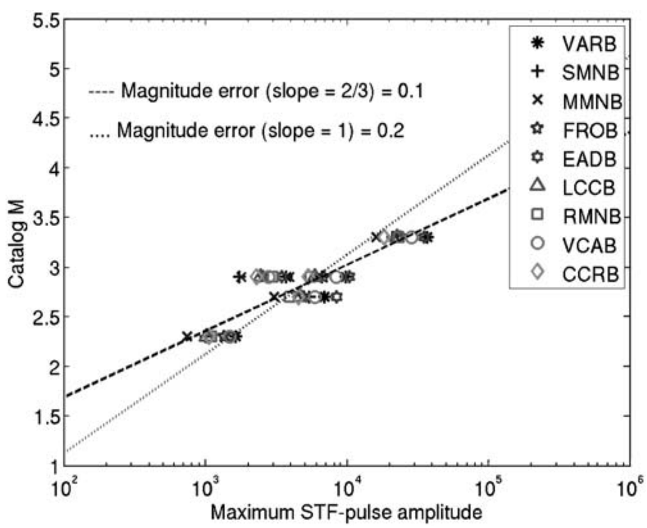

Figure 3. Peak amplitude of the source time function determined by spectral deconvolution for a subset of events with epicenters in the middle of the seismic array having the same empirical Green's function versus NCSN catalog magnitudes at nine stations with good signal-to-noise ratios. The dotted line represents $M \propto \log(\mathrm{Amplitude})$, and the dashed line represents $M \propto 2/3 \log(\mathrm{Amplitude})$ (see text for discussion). The figure confirms the reliability of NCSN magnitude values, as the trend shows increasing amplitude with increasing catalog M.

$$M \propto \log(A). \quad (5)$$

The relationship in equation (5) is plotted as the dotted line in Figure 3. If the duration is independent of magnitude, then the slope would be 2/3 (dashed line) (from equations 2–4). The least-squares fit of the data to the line with a slope of 2/3 has an error of 0.1 magnitude units, and the fit of the line with a slope of 1 has an error of 0.2 magnitude units. Both fits have errors less then 10% of the smallest catalog magnitude values in the subset, suggesting that the catalog magnitudes are adequate proxies for the seismic moments of these events regardless of the scaling relationship considered. We discuss why it might be more appropriate to consider earthquakes on the San Andreas fault following a slope of 2/3 (fixed duration) in Figure 3 in the Source Duration Observations section.

Nearly all of the reported catalog magnitudes in our data set are duration magnitudes (Eaton, 1992). To address the accuracy of the catalog magnitude values, Eaton (1992) performs an extensive test on the reliability of the magnitudes determined by the Northern California Seismic Network that is consistent with the results of the smaller scale test in Figure 3. He reports average station magnitude residuals that are virtually independent of distance from the epicenter up to 800 km. All of our stations are located within approximately 30 km or less from the epicenters. He reports that all coda magnitudes and S-wave magnitudes are on average within 0.04 magnitude units of 293 local magnitudes calculated by University of California, Berkeley. Furthermore, Hanks and Kanamori (1979) suggest that local magnitude (M_L) scales with moment identically to moment magnitude (M_w), and Bakun (1984) shows that duration magnitude values determined in central California are consistent with local magnitude values. We therefore rely on the catalog magnitudes to determine the seismic moment (M_0) using the standard relation of equation (4).

Source Duration Observations

The difference between pulse widths for earthquakes both on and off of the San Andreas fault suggests that there is something different about the earthquakes on the fault. The source durations as determined from the stacked source time pulse half-widths (i.e., the pulse width at the amplitude equal to 1/2 of the peak amplitude) also indicate that the duration of the on-fault earthquakes varies little with magnitude. For example, Figure 4a,b,c indicates that the pulse width does not vary for earthquakes on the fault, suggesting that τ does not vary, with the exception of one outlier in Figure 4a.

In contrast, Figure 4d suggests that off-fault pulse widths become wider with increasing magnitude, which is what one would expect for constant stress drop. Our group of off-fault events has only 11 events but suggests consistency with a global observation of increasing duration with moment (see Kanamori and Brodsky, 2004, fig. 10).

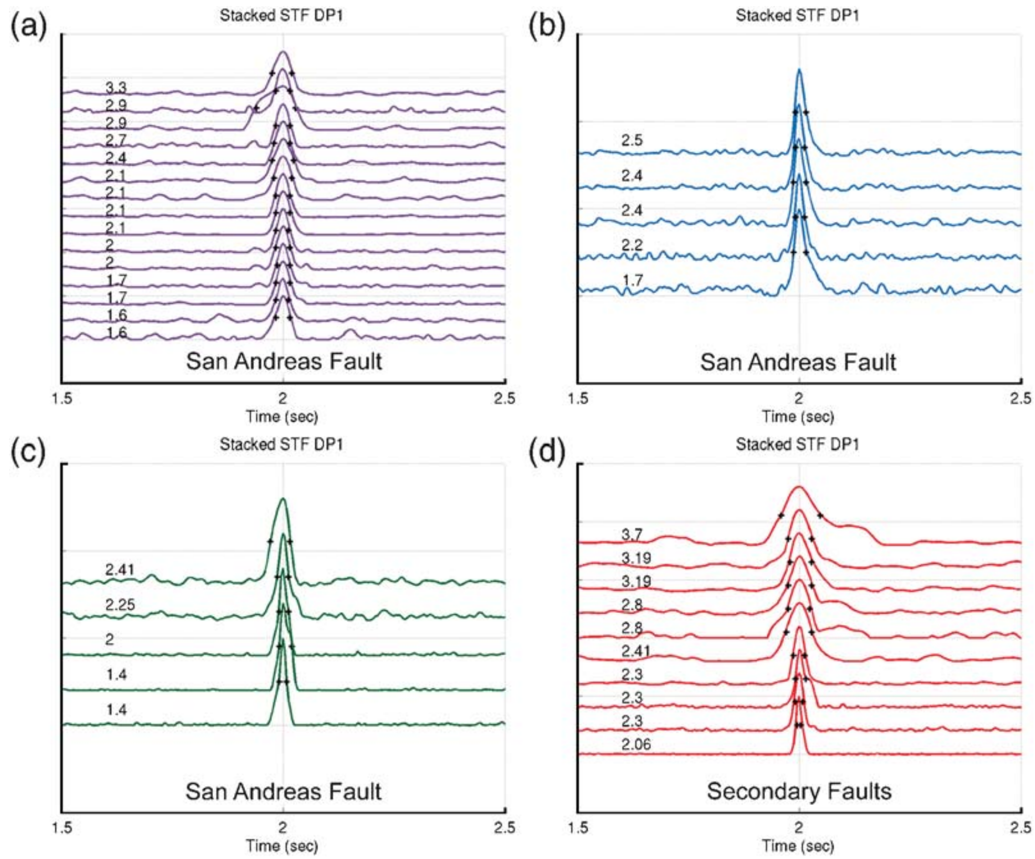

Figure 4. Source time functions (a–c) from the stacked vertical components of available stations for each individual earthquake located on the San Andreas fault, and (d) on secondary faults. (a), (b), and (c) correspond to the purple, blue, and green symbols, respectively, in Figure 2; (d) corresponds to the red and orange symbols in Figure 2. The earthquakes in (d) occur at a variety of locations. Asterisks note the limits of the pulse width at 1/2 the peak pulse amplitude. Each pulse is normalized in amplitude, and the catalog magnitudes are indicated on the left-hand side.

However, the fact that the source durations of the on-fault events do not vary with magnitude suggests a problem regarding the empirical Green's function approach. In order to use spectral deconvolution to obtain the source time function, one must be able to assume that the source spectra of the smaller event is flat in comparison to the larger event in the frequency band being analyzed. The assumption means that the spectral corner of the small event must be at a sufficiently high frequency beyond the spectral corner of the larger event in order to resolve the high frequencies of the larger earthquake. For typical source scaling, this means the smaller event should be at least an order of magnitude smaller (Nakanishi, 1991; Hough, 1997; Lanza *et al.*, 1999; Prieto *et al.*, 2004).

Figure 4 suggests that either the on-fault events do not obey source scaling (in this case have a nearly constant duration) or that there is potentially a problem with the deconvolution. If the events in our data set have a constant source duration and therefore have spectral corners with similar frequencies, then we would obtain source time functions with similar widths over a range of magnitudes, as seen in Figure 4. This means that the flat-spectral assumption may not apply and that the source time functions calculated from a spectral deconvolution approach might be unreliable. Examination of the raw pulse widths between the main events and empirical Green's functions (i.e., numerators, and denominators used in the spectral division) suggests that the durations of the smaller events range between 20% and 40% smaller than the larger event durations. In order to verify whether the difference is sufficient, we calculate the durations as measured from the width of direct P-wave arrival at the zero crossing in the raw waveforms and compare the results to the spectral deconvolution results.

An example of the source durations determined at one station is shown in Figure 5. The pulse width plots for other stations look similar to the examples shown. The P-wave pulse width was measured at all stations, and the duration for each event is taken as the average width. We use the raw waveform in order to insure that we do not consider any oscillations at the beginning of the earthquake signal resulting from deconvolving the instrument response mistakenly as a P-wave arrival. Furthermore, by using the direct P arrival, we mitigate any possible effects of fault-guided waves, given that they travel much more slowly than the direct P waves (Li *et al.*, 1997).

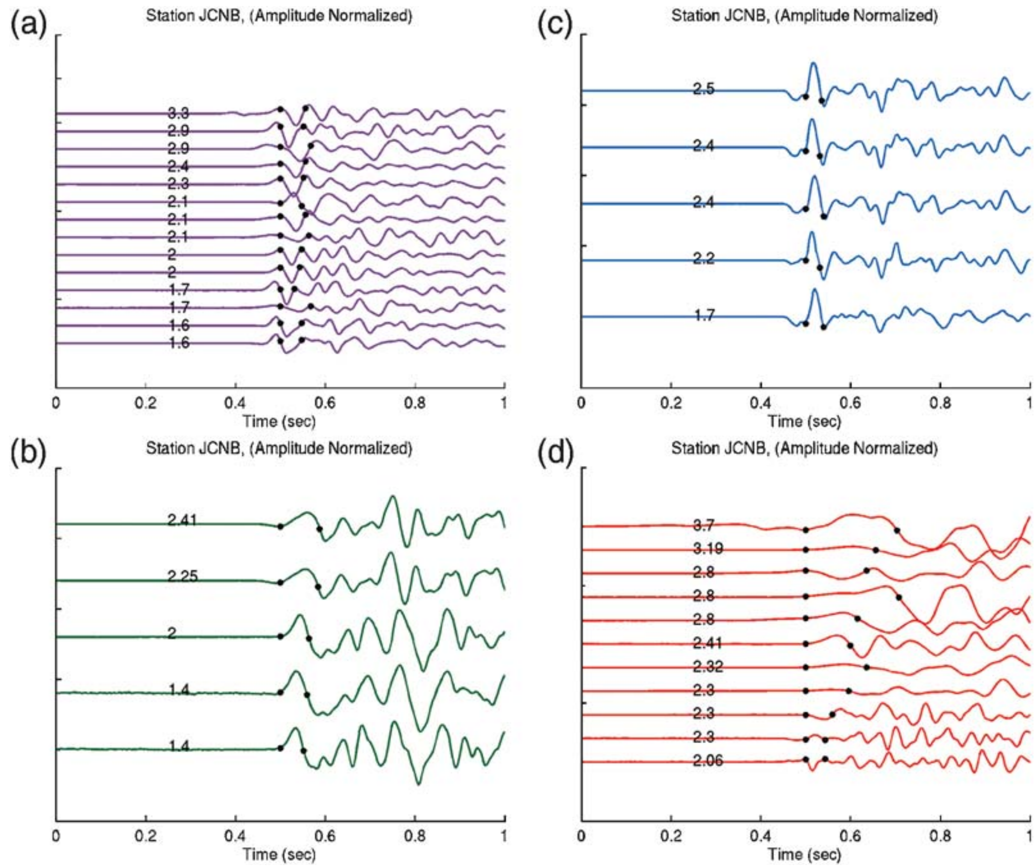

Figure 5. Pulse width measurements of the direct P-wave arrival in the cluster of earthquakes at station JCNB (a) southeast of the HRSN array, (b) middle of the array, (c) northwest of the array, and (d) on secondary faults. Pulse width measurements at other stations look similar. Earthquakes in (a), (b), and (c) are located on the San Andreas fault. The raw data traces are normalized and colored according to colors shown in Figure 1. Asterisks note the limits of the pulse at the zero crossing on the time axis.

The durations measured from direct P-wave arrivals confirm that the durations of the on-fault events do in fact vary only slightly with moment (Fig. 6). In the case of constant stress drop, the expected relationship between duration and moment would be $\log(\tau) \propto \frac{1}{3}\log(M_0)$. However, a least-squares fit to the on-fault duration/moment values suggests a slope much closer to zero (namely $\log(\tau) \propto \frac{3}{50}\log(M_0)$).

We estimate the error in the pulse width value for each earthquake via a jackknife standard error calculation. The error estimation consists of calculating the mean pulse width for each earthquake measured at all stations with one removed and repeating the calculation each time with a different station removed to create a set of pulse width values. The jackknife standard error is then calculated from the standard error of the set of pulse width values calculated with the reduced data set. Figures 6 and 7 imply the validity of the spectral deconvolution approach, given that it produces the same relationship between moment and duration as the method determining duration via the direct P-wave arrival, which incorporates no assumptions about the data. The particularly large error bar on the off-fault earthquake (with moment value near 2×10^{13} N m) in Figure 7 results from the fact that the empirical Green's function of the earthquake was measured at only three stations.

We now explain why we might expect the earthquake amplitudes to follow a slope of $2/3$ shown by the dashed line in the logarithmic plot of Figure 3 rather than the slope of 1 shown by the dotted line. Consider once again the relationship between source time function amplitude and the moment rate in equation (2). Figure 4 indicates that the duration is constant, and we would therefore expect τ in equation (2) to be constant.

With τ constant, and using the relation given in equation (4), we can determine the expected relationship of amplitude and magnitude for a constant earthquake duration,

$$A \propto M_0 \Rightarrow M \propto 2/3\log(M_0) \propto 2/3\log(A). \qquad (6)$$

The smaller error of the least-squares fit of the line with the slope of $2/3$ suggests that the data do in fact follow the normal $2/3$ slope more closely. Following the $2/3$ slope is consistent with the observation of nearly constant duration for the on-fault events.

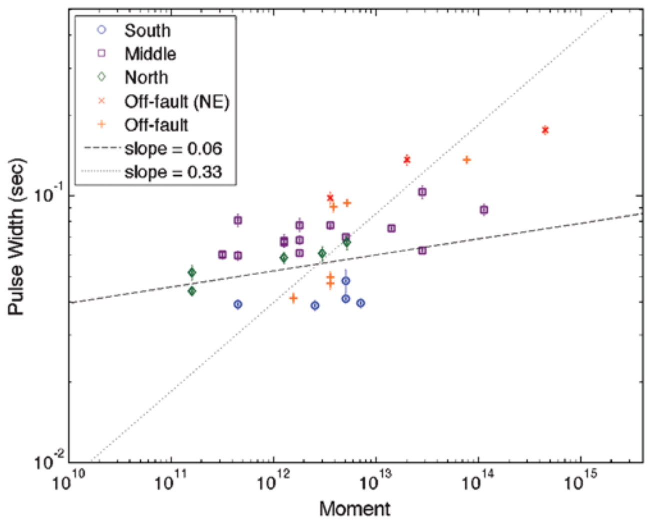

Figure 6. Source duration versus seismic moment for on-fault (blue circles, purple squares, and green diamonds) and off-fault (orange crosses and red Xs) events used in our study. The nearly constant durations in Figure 4 call the spectral deconvolution approach into question, as the spectra of the smaller events cannot be assumed to be flat. Therefore, we measure the earthquake durations from the width of the P arrival at the zero crossing of the time axis in the raw waveform as well. The observed relationship between moment and duration is consistent with that observed via the spectral deconvolution method (Fig. 7). Error bars indicate the standard deviation determined from a jackknife measure of standard error (see text). The dotted line represents the expected scaling for a constant stress drop (seen in the off-fault events), and the dashed line represents the scaling observed for the on-fault events (see text). The slope of the dashed line is determined via a least-squares fit to the on-fault moment/duration values.

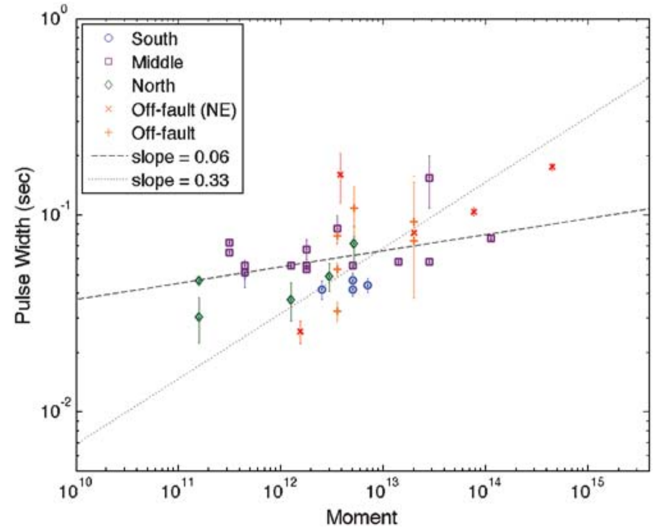

Figure 7. Source duration versus seismic moment for on-fault (blue circles, purple squares, and green diamonds) and off-fault (orange crosses and red Xs) events used in our study. We measure the earthquake durations from the 1/2 width of the source time function pulse. The observed relationship between moment and duration is consistent with that observed via the direct P arrival. Error bars indicate the standard deviation determined from a jackknife measure of standard error, which excludes one station for each pulse width calculation. The dotted line represents the expected scaling for a constant stress drop (seen in the off-fault events), and the dashed line represents the scaling observed for the on-fault events (see text). The slope of the dashed line is determined via a least-squares fit to the on-fault moment/duration values.

Source Spectral Observations

The source time spectra of the off-fault earthquakes imply distinctive differences in spectral shape between the off-fault and on-fault earthquakes as well (Fig. 8). The on-fault events all have relatively similar durations, and therefore similar corner frequencies, despite the variation in M_0 (given that $f_c \propto \frac{1}{\tau}$).

In contrast, the corner frequencies of the off-fault events follow more closely the expected relationship between M_0 and f_c^{-3} if $\Delta\sigma$ is constant, namely $M_0 \propto f_c^{-3}$ (Fig. 9) (Abercrombie, 1995; Ide *et al.*, 2003; Prieto *et al.*, 2004; Abercrombie and Rice, 2005; Imanishi and Ellsworth, 2006). For example, note the similarity to the plot of M_0 versus f_c^{-3} in Figure 10. The figure shows the same relationship measured on what is known to be a nascent fault surface at Mount St. Helens (Harrington and Brodsky, 2007). The fault is in new rock formed by a volcanic eruption that is subsequently faulted. The earthquakes represented in Figure 10 are analogous to the off-fault earthquake population because both groups occur on faults with little cumulative slip. Furthermore, in the cases where an individual cluster on the secondary fault system has a spread of magnitudes, the range of magnitudes represents a range of corner frequencies more closely following the f_c^{-3} scaling than the constant f_c scaling (red Xs in Fig. 9). Therefore, the scaling of corner frequencies, even within a cluster, is different on the secondary faults than on the main strand of the San Andreas fault.

The durations of the on-fault events remain roughly the same over the range of M_0 used in this study, suggesting that earthquakes in the magnitude range seen here on the fault have similar duration, regardless of size. The lack of variation in τ (and hence in f_c) has implications for $\Delta\sigma$, which we detail in the Discussion section.

Discussion

Duration

Source duration is proportional to rupture velocity, V, and fault length, or $S^{1/2}$, where S is fault area. Some physical model may exist that would require V to vary with magnitude. However, to explain our observations, such a model would exactly require that V and the fault length trade off in such a precise way as to keep the source duration nearly constant. We therefore argue by Occam's Razor that there is no reason to assume such a specific systematic change in V with magnitude and that an unchanging duration is better explained as an unchanging fault area.

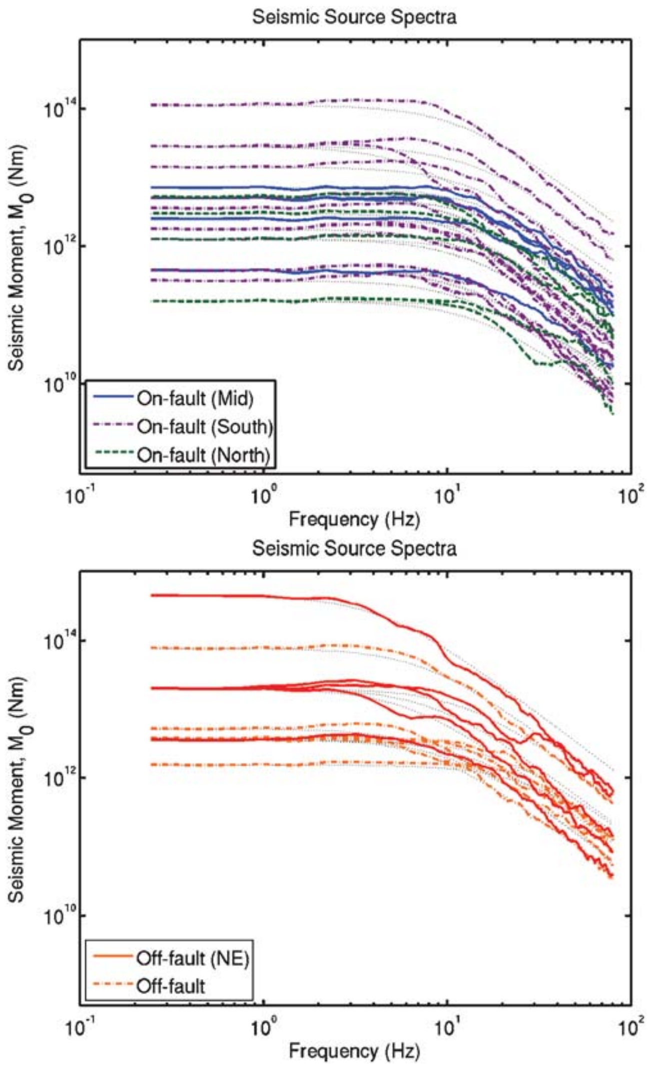

Figure 8. Off-fault (red and orange curves) and on-fault (purple, blue and green curves) source spectra determined from spectral deconvolution of a smaller, colocated event. The figure shows plots of the catalog seismic moment versus frequency. The finely dotted lines indicate the least-sqaured Brune spectral fit (equation 1).

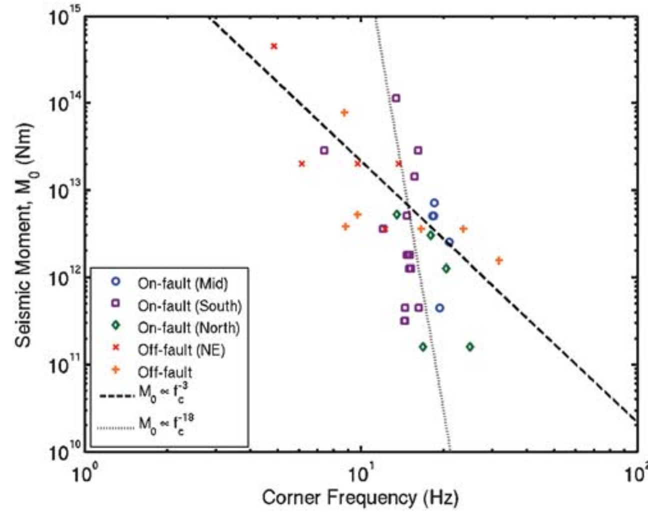

Figure 9. M_0 versus corner frequency, f_c, as determined by a least-squares fit to a Brune spectrum (equation 1). Symbols follow the color scheme shown in Figure 2. All off-fault events in the cluster northeast of the fault labeled "Off-fault (NE)" (red Xs, Fig. 2) likely occur on the same fault, suggesting that individual secondary faults have earthquakes with a variety of durations. The dashed line indicates the theoretically expected relationship of $M_0 \propto f_c^{-3}$, assuming a constant stress drop. The dotted line indicates the least-squares fit to the off-fault events. The difference in slope between the dashed and dotted lines illustrates the deviation of the on-fault events from the constant stress-drop case.

Therefore, the nonvarying source duration of the events on the San Andreas fault suggests that all of the $M \leq 3.3$ earthquakes have the same fault area and that differing amounts of average slip on the fault dictate the change in M_0 (Fig. 4). A constant S also implies that changes in average slip are solely responsible for changes in $\Delta\sigma$ (equation 9).

Spectral Data ($\Delta\sigma$)

The source durations, and hence the corner frequencies of the earthquakes on the San Andreas fault, do not vary with M_0. Although the data set contains fewer earthquakes on secondary faults, they obey a scaling suggestive of a constant stress drop commonly observed over a wide range of studies (Ide *et al.*, 2003; Prieto *et al.*, 2004; Abercrombie and Rice, 2005; Shearer *et al.*, 2006, e.g.), and we therefore emphasize the more uncommon lack of M_0/τ scaling for the earthquakes on the San Andreas fault. Using M_0 and f_c values, we calculate the stress-drop values for the earthquakes in our data set using the following relation:

$$\Delta\sigma = \frac{7M_0}{16}\left(\frac{0.32\beta}{f_c}\right)^3, \tag{7}$$

where β is the shear velocity, which we approximate at 3500 m/sec, and fault radius is written in terms of corner frequency, assuming a constant rupture velocity (Kanamori and Anderson, 1975; Madariaga, 1976). Using this relation to calculate stress drop, we get values of $0.18 \leq \Delta\sigma^{\text{on}} \leq 63$ MPa for the earthquakes on the San Andreas fault and of $0.31 \leq \Delta\sigma^{\text{off}} \leq 14$ MPa for earthquakes on secondary faults (Fig. 11). The roughly constant duration of the on-fault events implies an increase in stress drop with moment.

Our events do not have constant recurrence intervals like those observed by Nadeau and Johnson (1998). All but three earthquakes in our data set occur following the 2004 Parkfield mainshock. The lack of constant recurrence interval in our data set might be the result of the nonconstant loading of the aftershock sequence. However, there is no obvious increase in the interevent time for each cluster over time. The earthquake locations in our data set also differ, suggesting that they are not the same events to which they refer (gray circles, Fig. 1). They are located in very close proximity, and therefore might be expected similarly to have unusual source characteristics such as those observed by Nadeau and Johnson (1998).

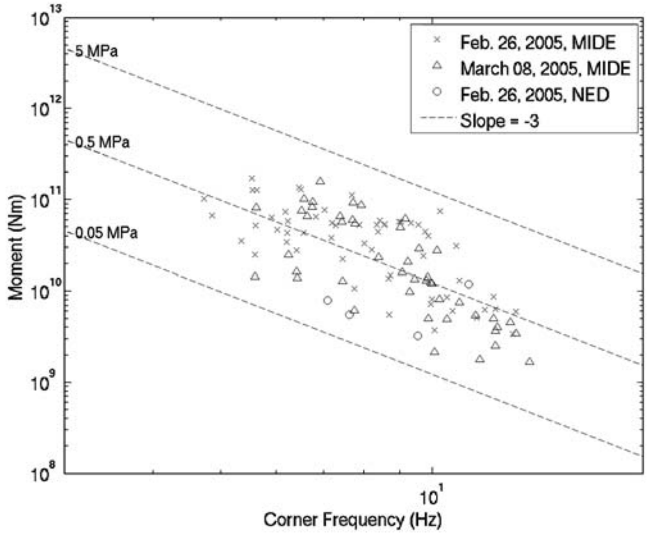

Figure 10. M_0 versus f_c as determined by a least-squares fit to a Brune spectrum (equation 1). Earthquakes occurred on a nascent fault surface in the dome of Mount St. Helens in February and March of 2005. The earthquakes shown are analogous to the off-fault earthquakes near Parkfield because they occur on faults with little cumulative slip. The figure shows that the trend of $M_0 \propto f_c^{-3}$ is a commonly observed relationship. The dashed lines indicate lines of constant stress drop and the range of commonly observed values (Abercrombie, 1995). The various symbols refer to the date and the station on which the earthquakes were recorded.

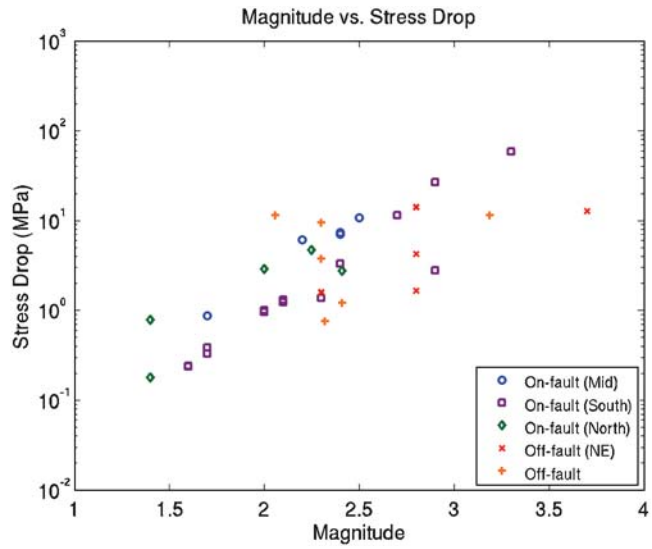

Figure 11. Seismic moment versus stress drop for earthquakes on the San Andreas fault (blue, cyan, and green symbols) and on secondary faults (orange and red symbols). The different symbols represent the different (clustered) locations of the events. The approximately constant duration of the on-fault events implies a decreasing stress drop with magnitude, in contrast with the constant stress drop shown here for the off-fault events. The stress-drop dependence on moment is a direct result of the lack of variation of source duration (and hence corner frequency) with moment.

The discrepancy in the stress drops measured by Nadeau and Johnson (1998) and our data set might readily be explained by their assumption that the cumulative seismic slip rate $\dot{d}$ is equal to the total geodetic slip rate. Within a given sequence of repeating earthquakes, they solve for the area of the fault on which the sequence occurs, given the total moment rate, $\dot{M}_0$, and the seismic slip rate based on the geodetic assumption, $\dot{d}$. The area within a given sequence is assumed to be constant because the magnitudes within a sequence do not vary. Therefore, the scalar equation for moment can be differentiated, and the measured values of moment and slip rate can be substituted to yield the area, S:

$$\dot{M}_0 = \mu S \dot{d}. \tag{8}$$

If some portion of the geodetic slip is aseismic, then $\dot{d}$ will be overestimated and the fault area will be underestimated. This will lead to an overestimation of stress drop, which might also be calculated using

$$\Delta\sigma \propto \mu \frac{\overline{d}}{S^{1/2}}, \tag{9}$$

where $\overline{d}$ refers to the average slip over the fault surface. Given that the repeating sequences occur in the creeping/locked transition zone of the fault, the assumption that the long-term slip rate is accommodated seismically is likely invalid, meaning that slip rate, and hence stress drops, would indeed be overestimated by Nadeau and Johnson (1998).

Interpretation

Our observations of earthquakes ranging over nearly two orders of magnitude on the San Andreas fault having a constant duration are consistent with a model of a strong asperity in a creeping fault. The constant duration observed for events on the fault is best explained by a repetitive rupture on a patch of unchanging area. If a single asperity ruptures repeatedly, then the fault area would not change. The fact that most earthquakes obey source scaling suggestive of constant stress drop implies that the events on the San Andreas fault are inherently different.

A speculative reason for this difference might be fault maturity. Recent observations of fault surface roughness suggest that faults become more smooth in the direction of slip with increasing cumulative slip (Sagy *et al.*, 2007). As faults accumulate more slip, the surfaces evolve seemingly through a continuum of degrees of surface roughness (Sagy *et al.*, 2007). We conjecture that as some fault surfaces change, properties of earthquakes might change as well. The San Andreas fault at Parkfield is a well-developed plate-boundary fault, with hundreds of kilometers of cumulative displacement (Wesnousky, 1990). It seems plausible that small earthquakes occurring here might have characteristic features in their source parameter relationships that differ from a collective data set of earthquakes from various types of faults. An additional factor differentiating the small earthquakes here is the fact that they occur in the transition zone between the creeping and locked portion of the San Andreas fault

(Titus *et al.*, 2005). Therefore, it is not entirely clear whether differences in source parameters result primarily from fault maturity or from the unique creeping/locked transition. A good test of this hypothesis would be to perform the same type of analysis for similar populations of earthquakes in another region. For example, southern California is also a well-instrumented area, where many faults of different degrees of cumulative slip are well characterized. In particular, seismicity rates near the ANZA network used by Prieto *et al.* (2004) are sufficiently high to provide a reasonable data set for comparison of source parameters (e.g., 470/800 earthquakes from 1983 to 1993 in a 4.5×4.5 km^2 area surpass their signal-to-noise ratio requirements).

On a broad scale, observations of stress drop are typically considered constant over many orders of seismic moment (Abercrombie, 1995; Ide *et al.*, 2003; Abercrombie and Rice, 2005; Imanishi and Ellsworth, 2006). However, the values of stress drop observed can typically vary over 3 orders of magnitude. Our study illustrates the merit of looking at differences between specific earthquake populations on a fine scale. Because the stress drops of the earthquakes on the San Andreas fault probably fall within the typical range, examining them in the context of a large regional data set would obscure their unusual features. The range in stress drop we observe for the particular area in this study suggests that at least some of the range in typical values may be the result of physical differences between various faulting environments, rather than simply scatter.

Conclusions

We compared the seismic sources of 25 earthquakes on the San Andreas fault and 11 earthquakes on secondary faults near Parkfield ranging in magnitude from 1.4 to 3.7. We find that the earthquakes occurring on the San Andreas fault have a constant duration over the magnitude range of our data set. In contrast, we reproduce the more usual source parameter scaling suggestive of a constant stress drop for the earthquakes on secondary faults. The constant source duration observation for the earthquakes on the San Andreas fault suggests that fault area stays constant over the magnitude range used, without invoking an unrealistic systematic change in rupture velocity that trades off with length.

The constant duration may be explained by a repetitive rupture of a small, locked asperity in a creeping fault. The dimensions of the asperity could predetermine the fault area, meaning that for the small earthquakes, all of the variation in seismic moment is determined by the slip. Therefore, changes in slip alone, rather than fault length, will dictate changes in stress drop. Where earthquakes are observed on secondary faults, slip and fault dimensions scale in a constant way, moment variation is determined by both, and stress drop does not vary.

Our calculations indicate stress-drop values ranging from 0.3 to 14 MPa for earthquakes on secondary faults, and values ranging from 0.18 and 63 MPa for earthquakes on the San Andreas fault. The stress-drop values fall within the accepted range for tectonic earthquakes. A comparison of stress drop versus seismic moment for the entire population of events in our data set might not be indicative of any characteristic scaling or lack thereof. The merits of performing this analysis in a restricted area with high-quality borehole data becomes evident when observing differences in the source scaling parameters of the two types of earthquake populations that become apparent when the populations are observed separately.

Data and Resources

Earthquake catalog data for relocated events preceding 2006 were obtained from the electronic supplement of Thurber *et al.* (2006). Catalog data from 2006 onward, as well as all waveform and station data from the HRSN, were obtained by searching the NCEDC Web site. The waveform data are public and provided by the Berkeley Seismological Laboratory, University of California, Berkeley. They are accessible via the following address: http://www.ncedc.org/ncedc/station.info.html (last accessed June 2008).

Acknowledgments

The projected Landweber deconvolution code was provided by Hiroo Kanamori. We would like to thank Thorne Lay for many insightful discussions that improved the quality of this manuscript. This work was supported by the National Science Foundation Grant Number EAR-0711575.

Reference

Abercrombie, R. E. (1995). Earthquake source scaling relationships from −1 to 5 $M(L)$ using seismograms recorded at 2.5-km depth, *J. Geophys. Res.* **100,** 24,015–24,036.

Abercrombie, R. E., and J. R. Rice (2005). Can observations of earthquake scaling constrain slip weakening?, *Geophys. J. Int.* **162,** 406–424.

Bakun, W. H. (1984). Seismic moments, local magnitudes, and coda-duration magnitudes for earthquakes in central California, *Bull. Seismol. Soc. Am.* **74,** no. 2, 439–458.

Brune, J. N. (1970). Tectonic stress and the spectra of seismic shear waves from earthquakes, *J. Geophys. Res.* **75,** 4997–5009.

Dreger, D., R. M. Nadeau, and A. Chung (2007). Repeating earthquake finite source models: Strong asperities revealed on the San Andreas fault, *Geophys. Res. Lett.* **34,** L23302.

Eaton, J. P. (1992). Determination of amplitude and duration magnitudes and site residuals from short-period seismographs in northern California, *Bull. Seismol. Soc. Am.* **82,** 533–579.

Hanks, T. C., and H. Kanamori (1979). A moment magnitude scale, *J. Geophys. Res.* **84,** 2348–2350.

Harrington, R. M., and E. E. Brodsky (2007). Volcanic hybrid earthquakes that are brittle-failure events, *Geophys. Res. Lett.* **34,** L06308.

Hough, S. E. (1997). Empirical Green's function analysis: Taking the next step, *J. Geophys. Res.* **102,** 5369–5384.

Ide, S., G. C. Beroza, S. G. Prejean, and W. L. Ellsworth (2003). Apparent break in earthquake scaling due to path and site effects on deep borehole recordings, *J. Geophys. Res.* **108,** 2271.

Imanishi, K., and W. L. Ellsworth (2006). Source scaling relationships of microearthquakes at Parkfield, CA, determined using the SAFOD pilot hole seismic array, in *Earthquakes: Radiated Energy and the Physics of Faulting*, R. E. Abercrombie, A. McGarr, H. Kanamori, and G. Di Toro (Editors), American Geophysical Monograph **170**, 81–90.

Kagan, Y. Y. (1997). Statistical aspects of Parkfield earthquake sequence and Parkfield prediction experiment, *Tectonophysics* **270,** 207–219.

Kanamori, H., and D. L. Anderson (1975). Theoretical basis of some empirical relations in seismology, *Bull. Seismol. Soc. Am.* **65,** 1073–1095.

Kanamori, H., and E. E. Brodsky (2004). The physics of earthquakes, *Rep. Prog. Phys.* **67,** 1429–1496.

Lanza, V., D. Spallarossa, M. Cattaneo, D. Bindi, and P. Augliera (1999). Source parameters of small events using constrained deconvolution with empirical Green's functions, *Geophys. J. Int.* **137,** 651–662.

Li, Y. G., W. L. Ellsworth, C. H. Thurber, P. E. Malin, and K. Aki (1997). Fault-zone guided waves from explosions in the San Andreas fault at Parkfield and Cienega Valley, California, *Bull. Seismol. Soc. Am.* **87,** 210–221.

Madariaga, R. (1976). Dynamics of an expanding circular fault, *Bull. Seismol. Soc. Am.* **66,** 639–666.

Nadeau, R. M., and L. R. Johnson (1998). Seismological studies at Parkfield VI: Moment release rates and estimates of source parameters for small repeating earthquakes, *Bull. Seismol. Soc. Am.* **88,** 790–814.

Nakanishi, I. (1991). Source process of the 1989 Sanriku-oki earthquake, Japan—source function determined using empirical Green's function, *J. Phys. Earth* **39,** 661–667.

Prieto, G. A., P. M. Shearer, F. L. Vernon, and D. Kilb (2004). Earthquake source scaling and self-similarity estimation from stacking *P* and *S* spectra, *J. Geophys. Res.* **109,** B08310.

Sagy, A., E. E. Brodsky, and G. J. Axen (2007). Evolution of fault-surface roughness with slip, *Geology* **35,** no. 3, 283–286.

Shearer, P. M., G. A. Prieto, and E. Hauksson (2006). Comprehensive analysis of earthquake source spectra in southern California, *J. Geophys. Res.* **111,** B06303.

Simpson, R. W., M. Barall, J. Langbein, J. R. Murray, and M. J. Rymer (2006). San Andreas fault geometry in the Parkfield, California, region, *Bull. Seismol. Soc. Am.* **96,** S28–S37.

Singh, S. K., and M. Ordaz (1994). Seismic energy release in Mexican subduction zone earthquakes, *Bull. Seismol. Soc. Am.* **84,** 1533–1550.

Thurber, C., H. Zhang, F. Waldhauser, J. L. Hardebeck, A. Michael, and D. Eberhart-Phillips (2006). Three-dimensional compressional wavespeed model, earthquake relocations, and focal mechanisms for the Parkfield, California, region, *Bull. Seismol. Soc. Am.* **96,** S38–S49.

Titus, S. J., C. DeMets, and B. Tikoff (2005). New slip rate estimates for the creeping segment of the San Andreas fault, California, *Geology* **33,** 205–208.

Venkataraman, A., L. Rivera, and H. Kanamori (2002). Radiated energy from the 16 October 1999 Hector Mine earthquake: Regional and teleseismic estimates, *Bull. Seismol. Soc. Am.* **92,** 1256–1265.

Wesnousky, S. G. (1990). Seismicity as a function of cumulative geologic offset: Some observations from southern California, *Bull. Seismol. Soc. Am.* **80,** 1374–1381.

Geophysikalisches Institut
Universität at Karlsruhe
Hertzstrasse 16
76187 Karlsruhe, Germany
rebecca.harrington@gpi.uni-karlsruhe.de
(R.M.H.)

Department of Earth and Planetary Sciences
University of California, Santa Cruz
1156 High Street
Santa Cruz, California 95060
brodsky@es.ucsc.edu
(E.E.B.)

Manuscript received 30 July 2008